COMMUNICATION

Engineering Polar Oxynitrides: Hexagonal Perovskite $BaWON_2$

Judith Oró-Solé,[a] Ignasi Fina,[a] Carlos Frontera,[a] Jaume Gàzquez,[a]Clemens Ritter,[b] Marina Cunquero,[c] Pablo Loza-Alvarez,[c] Sergio Conejeros,[d] Pere Alemany,[e] Enric Canadell,[a] Josep Fontcuberta,*[a] and Amparo Fuertes*[a]

Abstract: Non-centrosymmetric polar compounds have important technological properties. Reported perovskite oxynitrides show centrosymmetric structures and for some of them high dielectric constants have been observed, ascribed to local dipoles induced by partial order of nitride and oxide. Here we report the first hexagonal perovskite oxynitride $BaWON_2$, that shows a polar 6*H* polytype. Synchrotron X-ray and neutron powder diffraction, and annular bright-field in scanning transmission electron microscopy indicate that it crystalizes in the non-centrosymmetric space group $P6_3mc$, with total order of nitride and oxide at two distinct coordination environments in cubic and hexagonal packed BaX_3 layers. Synergetic second order Jahn-Teller effect supported by first principle calculations, anion order and electrostatic repulsion between W^{6+} cations induce large distortions at two inequivalent face sharing octahedra that lead to long-range ordered dipoles and spontaneous polarization along the *c* axis. The new oxynitride is a semiconductor with a band gap of 1.1 eV and a large permittivity.

Non-centrosymmetric compounds are pivotal in advanced applications such as actuators and sensors, data storage and computing, non-linear and non-reciprocal optics or photovoltaics.[1] In the search of non-centrosymmetric structures, transition metals with d^0 configurations in octahedral coordination have attracted attention because they may suffer distortions caused by electronic effects -e.g. second order Jahn-Teller effect (SOJT)-, often showing asymmetric environments and off-center displacements that lead to large dielectric constants and polar materials.[2] Anisotropic bond network, electrostatic repulsions and lattice stress reinforce the structural distortions,[3] and the existence of different anions in an ordered arrangement provide further sources of bond asymmetries and the possibility to create permanent dipoles and acentric structures.[4]

Perovskite oxynitrides ABO_2N or $ABON_2$ (*A*=rare earth or alkaline earth metal; *B*=transition metal) are important heteroanionic materials that show high dielectric constants and ferroelectricity among other relevant properties.[5,6] Large room-temperature dielectric constants (ε_r) have been reported for $BaTaO_2N$, $SrTaO_2N$ and $LaTiO_2N$, of 320-620,[7] 450[8] and 750 respectively.[9] Piezoelectric measurements showed fingerprints of ferroelectricity in epitaxial films of $SrTaO_2N$[10] and $BaTaO_2N$ crystals.[11]

All previously reported perovskite oxynitrides show centrosymmetric structures derived from the *Pm*-3*m* cubic aristotype, with symmetry lowering for Goldschmidt tolerance factors (t) below 1.[5] Reported tungsten perovskite oxynitrides are $RWO_{3-x}N_x$ (*R*=rare earth)[12,13] and $SrWO_2N$[14], with *t* values between 0.927 and 0.989. In pseudocubic perovskites all anion sites show similar coordination environments with cations, favouring total disorder of nitrogen and oxygen or partial order with local cis configuration of *B*-N bonds.[15] The origin of ferroelectricity in tantalum and titanium perovskite oxynitrides is still under discussion, and large dielectric polarizability is ascribed to the presence of randomly oriented local dipoles induced by the cis order of nitrides in the BO_4N_2 octahedra.[9, 10, 16]

In the quest for polar oxynitrides, a suitable strategy is to look for structures combining SOJT, octahedral d^0 transition metals and anion positions with well differentiated environments that could promote total order of N^{3-} and O^{2-}. Hexagonal perovskites ABX_3 formed by sequences of cubic and hexagonal close packing of AX_3 layers show two different environments for anions; those positioned in hexagonal packed layers are in sharing faces of the octahedra, while anions in cubic packed layers are in sharing corners. Face sharing BX_6 octahedra often show distortions because of *B*-*B* repulsions. These perovskites are stabilized for $t>1$, and the majority of reported compounds are formed by the large alkali or alkaline earth cations such as Ba^{2+} at the *A* site and transition metals at *B* sites.

The high charge of anion nitride stabilizes high oxidation states of the transition metal, and the combination of Ba^{2+} with highly charged small cations such as W^{5+} or W^{6+} predicts large tolerance factors, i.e. 1.052 and 1.058 for $BaWO_2N$ or $BaWON_2$ respectively, compatible with a hexagonal perovskite. Here we report the new compound $BaWON_2$ that is the first example of a hexagonal perovskite oxynitride. It is non-centrosymmetric and shows the 6*H* polytype, formed by cubic (*c*) packed BaN_3 layers and hexagonal (*h*) packed BaO_3 layers stacked in the sequence *cchcch* (Figure 1a). The new perovskite is a semiconductor, with band gap of about 1.1 eV, and shows a high dielectric constant ascribed to the presence of inequivalent octahedral *B* sites with distortions induced by SOJT effect and electrostatic repulsions between W^{6+} cations.

Powder samples of $BaWON_2$ were prepared starting either from mixtures of stoichiometric amounts of $BaCO_3$ and WO_3 or from $BaWO_4$, by treatment under flowing NH_3 at 750-800 °C. Experimental details are reported in the Supporting Information (SI). EDX analyses gave Ba:W ratios between 0.97 and 1.04, and N contents determined by combustion analysis were within 1.89-

[a] Dr. J.Oró-Solé, Dr. I.Fina, Dr. C.Frontera, Dr. J.Gàzquez, Prof. E.Canadell, Prof. J.Fontcuberta, Prof. A.Fuertes
Institut de Ciència de Materials de Barcelona(ICMAB-CSIC)
Campus UAB, 08193 Bellaterra(Spain)
E-mail: fontcuberta@icmab.cat
E-mail: amparo.fuertes@icmab.es
[b] Dr. C.Ritter
Institut Laue-Langevin, 71 Av. de Martyrs, Grenoble 38000(France)
[c] M.Cunquero, Dr. P.Loza-Alvarez
ICFO-Institut de Ciències Fotòniques, The Barcelona Institute of Science and Technology, Castelldefels (Spain)
[d] Dr. S.Conejeros
Departamento de Química, Universidad Católica del Norte, Av. Angamos 0610, Antofagasta 124000(Chile)
[e] Prof. P.Alemany
Departament de Ciència de Materials i Química Física and Institut de Química Teòrica i Computacional (IQTCUB), Universitat de Barcelona, Martí i Franquès 1, Barcelona 08028(Spain)

Supporting information for this article is given via a link at the end of the document.

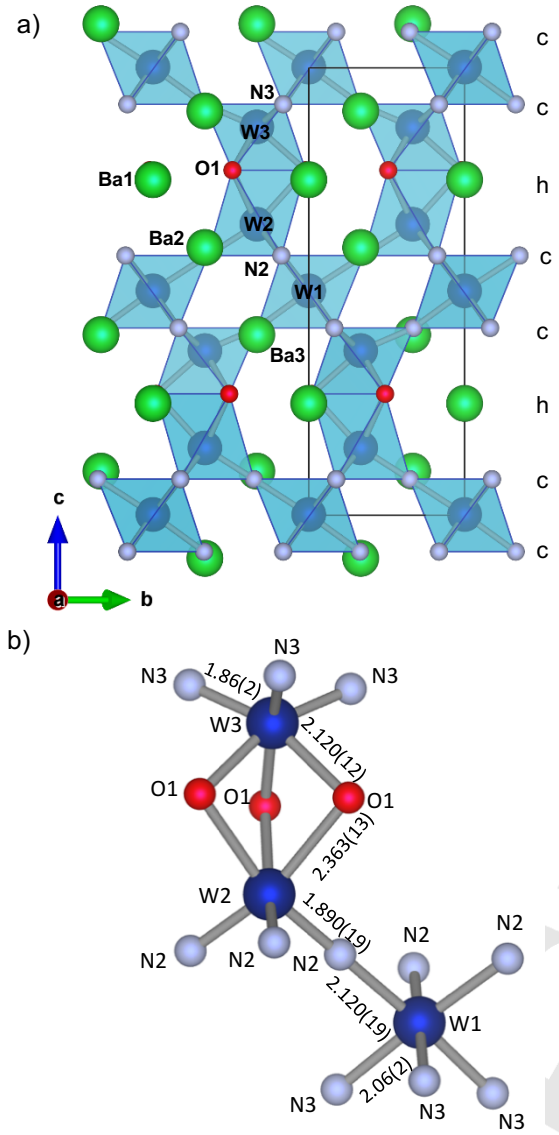

Figure 1. Crystal structure of $BaWON_2$: a) Projection along *a*-axis showing the sequence of hexagonal (*h*) and cubic (*c*) close packed BaO_3 and BaN_3 layers respectively in the 6H polytype. b) Coordination environment of W atoms.

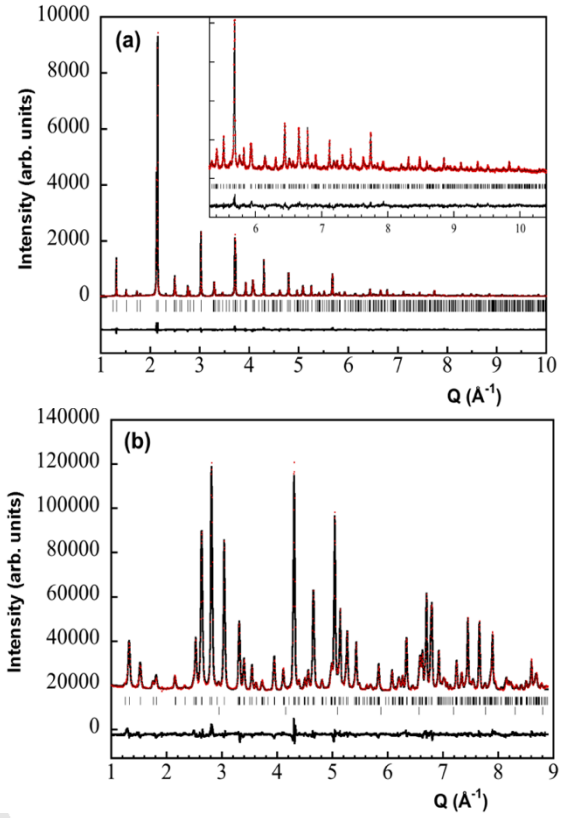

Figure 2. Rietveld fits to room temperature a) SXRD and b) ND patterns in $P6_3mc$ space group for $BaWON_2$ and $BaWO_{1.11}N_{1.89}$ respectively. The inset in (a) shows the high 2θ region enlarged.

2.13. N excess from the stoichiometric content in some samples can be ascribed to residual nitrogen-rich impurities not detected by X-ray powder diffraction. Rietveld refinement to synchrotron X-ray powder diffraction (SXRD) data was performed for the $BaWON_2$ composition using the structural models of the 6*H* hexagonal perovskite in the non-centrosymmetric $P6_3mc$ (N° 186) and in centrosymmetric $P6_3/mmc$(N° 194) space groups, that are compatible with reflection conditions determined by electron diffraction(See SI). The refinement in $P6_3mc$ (Figure 2a, Table S1) lead to cell parameters a=5.85073(2) and c=14.53220(9) Å with agreement factors R_{Bragg}=3.90% and R_{wp}=6.19%, whereas refinement using the space group $P6_3/mmc$ lead to poorer residuals, R_{Bragg}= 4.41% and R_{wp}= 6.47%. Refinement to neutron diffraction data (ND) of a ≈300 mg sample with 1.89 nitrogens per formula (Figure 2b, Table S3) was performed to investigate the anion distribution. This lead to smaller cell parameters (a= 5.84618(11), c= 14.3845(6) Å), which is consistent with the lower N/O ratio of this sample, and also showed better agreement factors in the $P6_3mc$ space group (R_{Bragg}=2.89%, R_{wp}=2.11%) than in $P6_3/mmc$ (R_{Bragg}=3.36%, R_{wp}=2.22%). N/O occupancies in $P6_3mc$ model were refined independently for the three 6*c* anion sites, resulting in an ordered distribution with full 1.0 oxygen occupancy at the site in hexagonal packed layers (*X*1), and N/O occupancies of 0.96(3)/0.04 and 0.94(3)/0.06 at the two sites of cubic layers *X*2 and *X*3 respectively. The refined N stoichiometry was 1.90 in excellent agreement with chemical analysis of the sample.

The $P6_3mc$ structure of $BaWON_2$ has three crystallographically independent positions for W in octahedral environments with C_3 axis distortions, located between hexagonal BaO_3 and/or cubic BaN_3 packed layers (Figure 1). W2 and W3 are placed at the face-sharing octahedra WO_3N_3 with *fac* configuration of nitride and oxide, and W1 is placed at the corner sharing octahedra WN_6. The WO_3N_3 octahedra show larger distortions (Δ_d as defined in [2] is 1.47 for W2 and 0.82 for W3) than that of the WN_6 octahedron (Δ_d=0.18), as a consequence of the repulsion between highly charged W^{6+} cations along the shared face, separated 3.161(8) Å. The distortion in the WO_3N_3 octahedra is enhanced by SOJT effect -also affecting the WN_6 octahedra- and by the higher covalency of the W-N bond compared to W-O bond. The preferred occupation of the more electronegative O atom at face-shared positions may be understood considering the weaker bonding for these sites with W-*X*-W angles ≈90°, compared with corner-shared sites, with W-*X*-W angles≈180°.[17] The spontaneous polarization, calculated from the coordinates and formal electrical charges of all atoms, is ≈17.7 μC/cm^2, parallel to the c axis. This value is lower than that estimated for $MnTaO_2N$ (55 μC/cm^2) with $LiNbO_3$-type structure.[18]

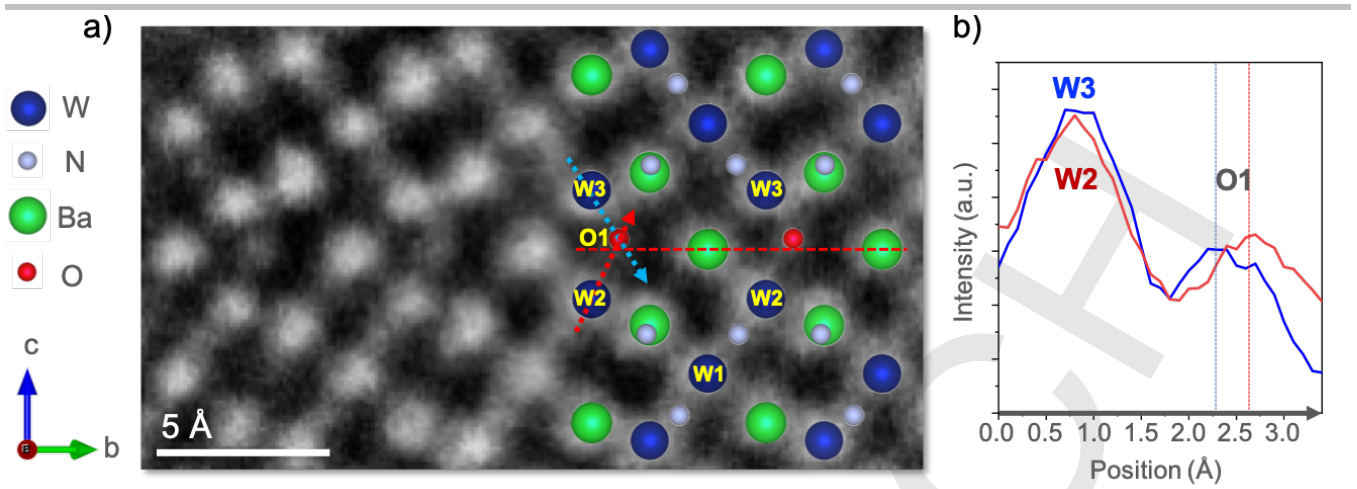

Figure 3. a) Atomic resolution contrast-inverted ABF image of $BaWON_2$ viewed along *a*-axis. The superimposed structure corresponds to the $P6_3mc$ model refined from SXRD. b) Intensity profiles drawn in a) along W2-O1 and W3-O1 directions. Vertical dashed lines mark the maximum of the intensity profile of O1 in each direction.

High-resolution aberration corrected annular bright field (ABF) images in scanning transmission electron microscopy allowed to map the position of all atoms including O and N columns in real space. The contrast-inverted ABF image of $BaWON_2$ along *a*-axis (Figure 3a) nicely matches the superimposed $P6_3mc$ structure determined from SXRD data. Oxygen atoms (O1) at *h* layers are shifted along *c* above Ba1 planes (horizontal dashed line), evidencing the acentric nature of the structure. Figure 3b, depicting the projected distances along W-O directions, clearly shows that W2-O1 bond (red profile) is longer than W3-O1 (blue profile), as determined from powder diffraction data (Figure 1b, Tables S1-S3).

The capability of $BaWON_2$ to generate a second harmonic generation (SHG) signal was assessed using a tunable Ti:sapphire ultrashort pulse laser as excitation source (details are reported at the SI) coupled to a nonlinear microscope. $BaWON_2$ powder was mixed with starch (wheat) that has been reported as an ideal SHG signal indicator. [19] Signals from the sample are filtered in the wavelength range corresponding to the SHG signal generated with the laser using a filter centered at 405 nm with a bandwidth of 10 nm. Under these conditions, we were able to obtain a signal of $BaWON_2$ that nicely mimics that generated by the reference sample (Figure 4a), suggesting that it arises from SHG conversion process. Recorded images were obtained from selected regions of the observed particles (Figures 4b and 4c). The fact that only regions of the particles could be imaged may result from their polycrystalline nature, implying that not all crystallites have the polar axis aligned with the polarization direction of the incoming light. Similarly, this may also imply that the sample itself highly absorbs the excitation or the generated wavelengths at different regions. To collect the recorded images, the required laser power was relatively large (~100 mW), which sometimes seemed to compromise the integrity of the sample.

The structure of $P6_3mc$ and $P6_3/mmc$ models of $BaWON_2$ was optimized using DFT calculations with the HSE06 functional [20] (details are reported in the SI). The $P6_3mc$ structure was found to be 3.4 kcal/mol more stable than $P6_3/mmc$. Whereas the centrosymmetric structure is semimetallic (Figure 5b), a band gap (indirect) of 0.64 eV opens in the polar structure (Figure 5a) because the two bands labeled with an asterisk (and degenerate at Γ) are pushed up when the mirror plane relating the face-sharing W octahedra (labelled W2 in the $P6_3/mmc$ model) is lost. These two bands are made of an out-of-phase combination of the pair of *e*-type *d* orbitals originating from the t_{2g} set of the distorted W2 octahedra (see in the inset in Figure 5b the illustration one of these two equivalent bands at Γ). The in-plane O p_x and p_y orbitals can only mix into these bands in the polar structure, while the mirror plane forbids mixing in the centrosymmetric structure. Since these bands are W-O antibonding and the W-O bonds are already long in the centrosymmetric structure, the stabilization afforded by the lengthening of one of these bonds is more than compensated by the destabilization due to the strengthening of the other bond. This is why the two bands are destabilized in the polar structure leading to a gap opening. These bands are empty and thus do not contribute to the total energy of the system, but exactly for the same reasons their two bonding counterparts (occurring within the sea of the occupied orbitals) are stabilized when the symmetry plane disappears and the O p_x and p_y orbitals mix into, thus increasing the W-O bonding. This second-order Jahn-Teller effect is thus responsible for the preference for the polar structure.

The temperature-dependent electrical resistivity ρ(T) of a sintered pellet of $BaWON_2$ (Figure 6a) indicates a semiconductor-like behavior, with ρ(300 K) ≈ 40 Ωcm and resistivity rapidly increasing upon lowering the temperature (ρ(90 K) ≈ 170 Ωcm). ρ(T) is better described by variable range hopping model (VRH)

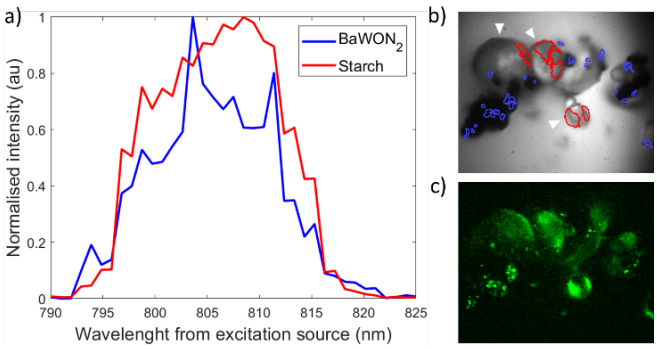

Figure 4. a) SHG signals obtained from $BaWON_2$ (blue) and starch granules (red) by scanning the excitation wavelength along the spectra of the Ti:sapphire laser. b) Transmission image of the starch granules (white arrow-heads) mixed with $BaWON_2$ powder. The regions analysed are marked in red and blue. c) Image obtained by using a filter centred at 405 nm.

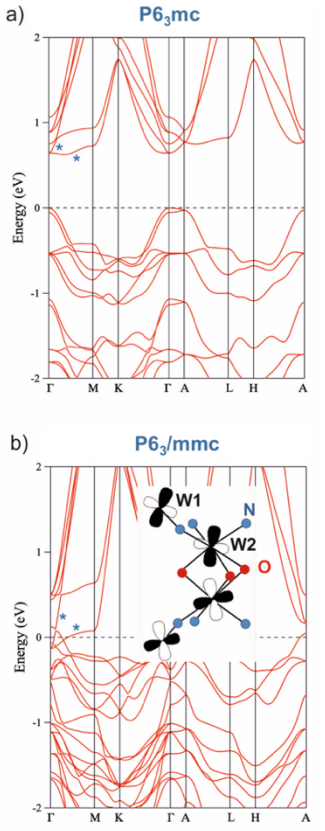

Figure 5. DFT band structure for optimized *P*6$_3$*mc* (a) and *P*6$_3$/*mmc* (b) crystal structures of $BaWON_2$. The inset in b) shows the nature of one of the two equivalent (at Γ) crystal orbitals in the *P*6$_3$/*mmc* model, noted with an asterisk.

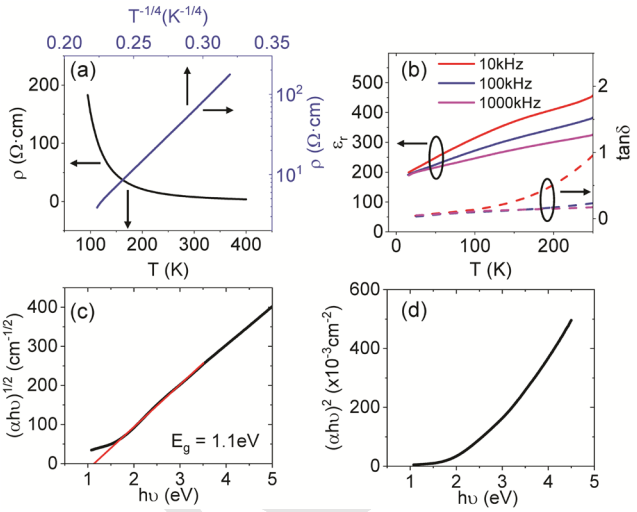

Figure 6. Temperature dependence in $BaWON_2$ of: (a) electrical resistivity ρ(T) (left axis) and ρ($T^{-1/4}$) (right axis). b) permittivity ε_r(T) and losses (tan δ) recorded at various frequencies. Optical absorption Tauc plots for (c) indirect and (d) direct transitions (d).

than by an Arrhenius law, suggesting that the motion of thermally activated carriers is limited by defects, prompting some localization and subsequent thermally stimulated hopping (VRH). The dielectric properties have been determined by impedance spectroscopy. Frequency-dependent permittivity (Figure 6b) shows that ε_r decreases when increasing frequency, signaling the contribution of a leakage-related resistive channel in the RC (resistance-capacitance) equivalent circuit of the measured sample. The strong frequency-dependent permittivity at high temperature is fully consistent with the corresponding ρ(T) data. The reduction of losses (tan δ) observed upon lowering temperature or increasing frequency (Figure 6b) is also fully consistent with a narrow band gap semiconducting material. The ε_r value (≈ 200–230 in the 10-100 K temperature range), is in line, although somewhat smaller, with values reported for $SrTaO_2N$. [21] The semiconducting behavior indicated by data in figures 6a and 6b is compatible with the observed black color of the samples. Optical absorption spectroscopic measurements were conducted on $BaWON_2$ powders diluted in KBr. Tauc plots for indirect and direct band absorption (Figures 6c and 6d) show that indirect transitions rule optical absorption, and the optical bandgap is about 1.1 eV. Both observations agree reasonably with DFT predictions.

To summarize, we have shown that compositional and steric design allows obtaining the new polar oxynitride $BaWON_2$, where oxide and nitride are ordered in two distinct coordination environments of the *6H* hexagonal perovskite structure. Anion order, together with electrostatic repulsion between W^{6+} cations, leads to anisotropic *M-X* bonds and high distortions of the face-sharing octahedra. Electronic effects are found to promote a second order Jahn-Teller distortion that lowers the energy of the $BaWON_2$ lattice, favoring a non-centrosymmetric structure by suppressing a mirror plane. As a result, a gap opens in the electronic band structure and a semiconducting ground state emerges, as confirmed by optical and electron transport data. The observed remarkably large permittivity is consistent with anisotropic, multi-anionic bond network in the structure, which in turn shall promote anharmonicity of the bond dynamics and subsequently the observed non-linear optical response. This achievement contrasts with earlier results on ABO_2N perovskites with pseudocubic centrosymmetric structures that lead to large dielectric permittivity and piezoresponse under electric field bias, ascribed to field-response of nanopolar regions, but without long range polar order. The relatively smaller permittivity of polar $BaWON_2$ compared to that of $BaTaO_2N$ is also consistent with this view. These findings show the potentiality of hexagonal perovskite oxynitrides as a new group of heteroanionic compounds to explore properties by considering different cation compositions, in particular for the search of polar materials, but also for important applications of oxynitrides such as visible light-active photocatalytic activity.

Acknowledgements

This work was supported by the Ministerio de Ciencia e Innovación, Spain (MAT2017-86616-R, MAT2017-85232-R, SEV-2015-0496, MDM-2017-0767, PGC2018-096955-B-C44 and PGC2018-093863-B-C22) and from Generalitat de Catalunya (2017SGR1377, 2017SGR581, 2017SGR1506 and 2017SGR1289). We thank Alba and ILL (experiments 2018082958 and 5-23-721,DOI: 10.5291/ILL-DATA.5-23-721) for beam time provision, and Dr. François Fauth for assistance in data collection at Alba. I.F and J.G. acknowledge the Ramon y Cajal contracts RYC-2017-22531 and RYC-2012-11709. S.C. was supported by FONDECYT, Chile (project 11107163). ICTS-CNME at UCM is acknowledged for offering access to STEM and expertise.

Keywords: oxynitrides • perovskite phases • polar materials• transition metals • hexagonal perovskites

References

[1] P.S.Halasyamani, K.R.Poeppelmeier, *Chem. Mater.* **1998**, *10*, 2753-2769.
[2] P.S.Halashyamani, *Chem. Mater.* **2004**, *16*, 3586-3592.
[3] M.Kunz, I.D.Brown, *J. Sol. State Chem.* **1995**, *115*, 395-406.
[4] H.Kageyama, K.Hayashi, K. Maeda, J.P. Attfield, Z.Hiroi, J.M.Rondinelli, K.Poeppelmeier, *Nat. Comm.* **2018**, *9*, 772.
[5] A.Fuertes, APL Mater. **2020**, *8*, 020903.
[6] Y.Kim, P.M.Woodward, K.Z.Baba-Kishi, C.W.Tai, *Chem. Mater.* **2004**, *16*, 1267-1276.
[7] A. Hosono, S-K. Sun, Y. Masubuchi, S. Kikkawa, *J. Eur. Cer. Soc.* **2016**, *36*, 3341-3345.
[8] S-K- Sun, Y-R. Zhang, Y. Masubuchi, T. Motohashi, S. Kikkawa, *J. Am. Ceram. Soc*. **2014**, 97, 1023-1027.
[9] D.Habu, Y. Masubuchi, S.Torii, T. Kamiyama, S. Kikkawa, *J. Sol. State Chem.* **2016**, *237*, 254-257.
[10] D. Oka, Y. Hirose, H. Kamisaka, T. Fukumura, K. Sasa, S. Ishii, H. Matsuzaki, Y. Sato, Y. Ikuhara, T. Hasegawa, *Sci. Rep.* **2014**, *4*, 4987.
[11] A.Hosono, Y.Masubuchi, S. Yasui, M. Takesada, T. Endo, M. Higuchi, M. Itoh, S. Kikkawa, *Inorg. Chem.* **2019**, *58*, 16752-16760.
[12] P. Antoine, R.Marchand, Y. Laurent, C. Michel, B. Raveau, *Mat. Res. Bull.* **1988**, *23*, 953-957.
[13] M. Yang, J.Oró-Solé, A. Kusmartseva, A. Fuertes, J.P. Attfield, *J. Am. Chem. Soc.* **2010**, *132*, 4822-4829.
[14] I.D.Fawcett, K.V.Ramanujachary, M.Greenblatt, *Mater. Res. Bull.* **1997**, *32*, 1565-1570.
[15] M. Yang, J. Oró-Solé, J.A. Rodgers, A.B. Jorge, A. Fuertes, J.P. Attfield, *Nature Chem.* **2011**, *3*, 47-52.
[16] J. Yamaura, S. Maki, T. Honda, Y. Matsui, A. Noviyanto, T. Otomo, H. Abe, Y.Murakami, N. Ohashi, *Chem. Commun.* **2010**, *56*, 1385-1388.
[17] T. Yamamoto, K.Shitara, S.Kitagawa, A.Kuwabara, M.Kuroe, K.IshidaM. Ochi, K. Kuroki, K.Fujii, M.Yashima, C.M. Brown, H.Takatsu, C.Tassel, H. Kageyama, *Chem. Mat.* **2018***, 30,* 1566-1574.
[18] C.Tassel, Y.Kuno, Y.Goto, T.Yamamoto, C.M.Brown, J.Hester, K.Fujita, M.Higashi, R.Abe, K.Tanaka, Y.Kobayashi, H.Kageyama, *Angew. Chem. Int. Ed.* **2015**, *54*, 516–521.
[19] I. Amat-Roldán, I. G. Cormack, P. Loza-Alvarez, D. Artigas. *Optics Let.* **2004**, *29*, 2282-2284.
[20] A. V. Krukau, O. A. Vydrov, A. F. Izmaylov, G. E. Scuseria, *J. Chem. Phys.* **2006**,*125*, 224106.
[21] S.Kikkawa, S.Sun, Y. Masubuchi, Y. Nagamine, T.Shibahara, *Chem. Mat.* **2016**, *28*, 1312-1317.

Entry for the Table of Contents

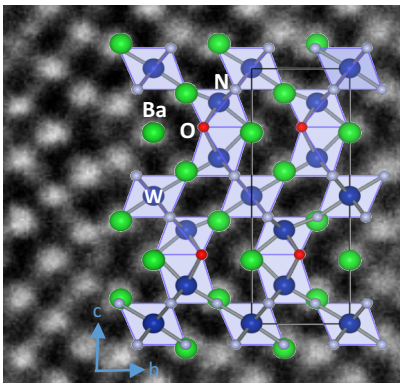

The new 6H hexagonal perovskite oxynitride $BaWON_2$ is a non-centrosymmetric polar compound that shows total order of nitrogen and oxygen in two distinct coordination environments. The combination of anion order, electrostatic repulsion between W^{6+} cations and second order Jahn-Teller effect induce different distortions at three inequivalent tungsten octahedra leading to long range ordered dipoles and spontaneous polarization along the c axis.